Iranian Polymer Journal (2020) 29:103–116
https://doi.org/10.1007/s13726-019-00778-4

ORIGINAL RESEARCH

Isothermal cold crystallization kinetics and properties of thermoformed poly(lactic acid) composites: effects of talc, calcium carbonate, cassava starch and silane coupling agents

Chutimar Deetuam[1] · Chavakorn Samthong[1] · Suphattra Choksriwichit[1] · Anongnat Somwangthanaroj[1,2]

Received: 5 July 2019 / Accepted: 28 December 2019 / Published online: 10 January 2020

Abstract
The effects of three different fillers (i.e., talc, calcium carbonate, and cassava starch) and surface functionalization by 3-aminopropyltriethoxysilane (APTES) and vinyltriethoxysilane (VTES) on morphology, thermal and tensile properties of the poly(lactic acid) (PLA) composites were comparatively examined. Dynamic differential scanning calorimetry (DSC) results revealed that the incorporation of filler can facilitate the cold crystallization of PLA, as confirmed by lowered cold crystallization temperature. By fitting DSC data with Avrami model, the highest isothermal cold crystallization rate constant k and the shortest crystallization half time $t_{1/2}$ were obtained for the PLA/talc composites under isothermal temperature of 100 °C, implying that talc was the most effective nucleating agent for PLA in this study. The average Avrami index n of neat PLA and its composites lay within the same range of 3.0–3.6, which reflected the three-dimensional spherulitic growth of PLA with the mixture of instantaneous nuclei and sporadic nuclei. In comparison with the composite cast films, the thermoformed films had higher degree of crystallinity as well as higher tensile strength and Young's modulus owing to the chain orientation upon annealing. Furthermore, the addition of silane-treated talc, especially APTES-treated talc, fastened cold crystallization rate and enhanced tensile properties because of the improved interfacial interaction between talc particles and PLA matrix.

Keyword Poly(lactic acid) · Silane treatment · Isothermal cold crystallization · Thermoforming · Tensile properties · Differential scanning calorimetry

Introduction

Considering the waste disposal crisis and global warming, biodegradable polymers have gained a great attention to replace the petroleum-based polymers because they can be synthesized from the abundant renewable resources (e.g., corn, potato, and sugarcane) and they can be enzymatically decomposed into CO_2, H_2O, and biomass in a short time [1, 2].

Poly(lactic acid) (PLA) is the most well-known biodegradable thermoplastic aliphatic polyester that has been extensively used for diverse applications, e.g., eco-friendly food packaging [3, 4] and drug delivery devices [5, 6] because of its unique properties including biodegradability, biocompatibility, high transparency, high tensile strength (75 MPa), and high tensile modulus (3.2 GPa) [7, 8]. Agricultural feedstock is converted into lactic acid monomer by bacterial or yeast fermentation, followed by ring-opening polymerization of lactic acid monomer into PLA. Nevertheless, PLA has several shortcomings such as high brittleness with elongation-at-break less than 4%, poor melt strength, poor thermal stability, and low gas barrier properties. Furthermore, PLA has slow crystallization rate leading to a very long processing cycle time and low crystallinity. As a result, the end-use packaging will have poor optical, thermal, and mechanical performances [9]. Annealing at isothermal temperature between glass transition temperature (T_g) and melting temperature (T_m) of polymer has been carried out to increase the crystallinity of the formed polymeric packaging; however, the final crystallinity of the unmodified PLA is still relatively

✉ Anongnat Somwangthanaroj
Anongnat.S@chula.ac.th

[1] Department of Chemical Engineering, Faculty of Engineering, Chulalongkorn University, 254 Phayathai Road, Patumwan, Bangkok 10330, Thailand

[2] Special Task Force of Activating Research (STAR) in Novel Technology for Food Packaging and Control of Shelf Life, Chulalongkorn University, Bangkok 10330, Thailand

low because of the intrinsically slow crystallization rate of PLA. From this reason, the crystallization rate of PLA must be improved for being used in some advanced applications requiring excellent thermal and mechanical properties.

Many studies have proposed that the incorporation of organic or inorganic fillers, e.g., organoclay [10, 11], alumina [12], cassava starch [13], titanium dioxide [14], and talc [15, 16], into the polymer matrix to create polymer composites. The aims of producing the polymer composites were to reduce price, enhance crystallization rate, shorten crystallization time, improve mechanical properties, and modify the gas permeability of the final polymer products.

Lule and Kim [12] prepared the PLA hybrid composites composed of 20 wt% alumina and 2 wt% aluminum nitride. The result showed that the hybrid fillers can enhance the crystallinity of PLA significantly, and the crystallinity of PLA improved from 22 to 50% by changing the type of filler from untreated alumina to maleic acid-treated alumina.

Petchwattana and Narupai [14] reported that the crystallization time to obtain half of overall crystallinity of PLA greatly reduced from 1620 to 59 s (96% reduction) with the addition of 3 wt% TiO_2 and further reduced to 18 s (99% reduction) when 3 wt% talc was incorporated into the PLA/TiO_2 nanocomposites. Moreover, the flexural modulus of all PLA composites was higher than that of the neat PLA because of the rigidity of talc and TiO_2, as well as, increased PLA crystallinity.

Nanthananon et al. [15] prepared the PLA-based hybrid composites containing short natural fiber and talc and it was found that the tensile strength and tensile modulus drastically increased with the incorporation of these fillers. Also, the relative crystallinity increased from 0.2% for virgin PLA to 9% and 33% with the addition of 30 wt% short natural fiber and 30 wt% talc, respectively.

In general, the compatibility between polymer matrix and filler particles was very poor; this resulted in poor stress transfer between polymer and filler across the interface, leading to poor mechanical performances of the polymer composites. To improve the interfacial interaction of polymer and filler, surface functionalization has been conducted to improve the polymer/filler compatibility [17]. Silanization has extensively been conducted in many polymer composites. Silane coupling agent comprises of two distinct reactive functional groups within the molecule; one of the functional groups (e.g., alkoxy groups) can be chemically bonded with the functional groups on the surface of inorganic filler while another organic functional group can chemically bond or interact with the polymer matrix. The included organic functional groups of silane coupling agent are not limited to epoxy [18], mercapto [19], methacrylate [20], vinyl [21, 22], or amino [23, 24] groups; but are dependent on the purpose and final targeted properties of the polymer composites.

Although the effects of talc, calcium carbonate ($CaCO_3$), and cassava starch on the properties of the PLA composites have been reported in many publications, to the best of our knowledge the comprehensive research has not been well reported on the comparison between these fillers as well as surface treatment by silane coupling agent. In this work, the effects of the addition of talc, $CaCO_3$, and cassava starch at various contents on the morphology, mechanical and thermal properties, and isothermal cold crystallization kinetics of the PLA composites were examined.

The isothermal cold crystallization kinetics was investigated by fitting the experimental data from the differential scanning calorimetry (DSC) with a theoretical Avrami model. The study on annealing at optimal cold crystallization temperature on the thermal and tensile properties was performed by comparing between cast films and thermoformed films. Eventually, surface treatments of talc with vinyltriethoxysilane (VTES) and 3-aminopropyltriethoxysilane (APTES) were also performed to examine the silanization effect on the properties of the PLA composites in comparison with the untreated system.

Experimental

Materials

Poly(lactic acid) (PLA) (grade: 2003D) containing ~ 96% *L*-lactic acid comonomer with a melt flow index of 6 g/10 min (210 °C/2.16 kg) was purchased from NatureWorks LLC, USA. Calcium carbonate ($CaCO_3$) and talc powders were supplied from Thai Chemical Industries, Thailand. Cassava starch flour was obtained from Thai Wah Food Products Public Company Limited, Thailand. The mean particle sizes of the pristine talc, $CaCO_3$, and cassava starch were 3, 5, and 12 µm, respectively. Fillers were used as received without modification unless otherwise specified. 3-Aminopropyltriethoxysilane (APTES, 98%) and vinyltriethoxysilane (VTES, 97%) as silane coupling agents were purchased from Sigma-Aldrich, USA. All solvents were in analytical grade and used as received without further purification.

Surface functionalization of filler

Surface functionalization of talc via silanization using APTES and VTES was performed to improve the dispersion of filler in the PLA matrix. Silane coupling agent was premixed with ethanol–water mixture (80:20 v/v) at concentration of 2% (w/v) for 1 h. Subsequently, pH of the solution was adjusted to 4.5–5.5 by adding acetic acid. In general, the silanization was carried out in acid-catalyzed condition to facilitate the hydrolysis rate of silane to silanol

and slow down the self-condensation of hydrolyzed silanols [25]. Talc, which was pre-dried at 60 °C overnight to remove moisture, was vigorously stirred in this acidic solution filled with silane coupling agent at room temperature for 2 h. Amount of silane was fixed at 2 wt% content of dried filler. Afterwards, treated talc was filtered and washed with distilled water several times to remove the untreated silanes. Finally, treated talc was dried at 60 °C in a vacuum oven until the constant weight was gained.

Preparation of the PLA composites

The PLA composites comprising of different filler types and contents (1, 3, 5, 7, and 10 vol%) were prepared. Fillers were dried in a vacuum oven at 60 °C overnight for moisture removal. PLA and filler were compounded using a co-rotating twin screw extruder ($L/D = 40$ and $D = 20$, Labtech Engineering, Thailand) operated at a mixing temperature of 165–180 °C and a screw speed of 50 rpm. The PLA composites were then casted into sheets by a co-rotating twin screw extruder (Thermo Haake, Rheocord 300p and Rheomex PTW 16/15 ($L/D = 15$ and $D = 16$ mm), Germany) equipped with a cast-film die (die gap = 1 mm) at a processing temperature of 130–185 °C and a screw speed of 80 rpm. Thickness of the cast sheets was around 400 µm.

Finally, sheets of PLA composites were thermoformed into 300 µm films at different isothermal conditions depending on the composite formulation using a laboratory thermoformed machine equipped with a vacuum apparatus. The annealing temperature and annealing time were decided from the DSC isothermal cold crystallization profiles in which annealing temperature was the isothermal temperature giving the fastest cold crystallization rate and annealing time was the overall crystallization time. These annealing conditions will be mentioned again in "Results and Discussion" section. Cast and thermoformed films of neat PLA were also prepared following the aforementioned procedure under the same condition. Therefore, neat PLA films were undergone under the same shear history and thermal history as those of the PLA composites. The nomenclatures of PLA composites are represented in Table 1.

Characterization

The surface functionalities of pristine and silane-treated talc particles were analyzed using Fourier transform infrared spectroscopy (FTIR, Thermo Scientific Nicolet 6700, USA) in a range of 400–4000 cm^{-1} with a resolution of ± 4 cm^{-1}. Crystalline potassium bromide (KBr) was used as a background. Predried talc (5 mg) was mixed with KBr pellet (400 mg) in an alumina mortar and pestle and the spectra of ground powder were characterized.

Morphology of the cross-sectional fractured surface of neat PLA and its composites was observed by a scanning electron microscope (SEM) (JEOL, JSM-6400, Japan) with an acceleration voltage of 8 kV. All cast film samples were fractured in liquid nitrogen and eventually coated with a

Table 1 Thermal properties of the neat PLA and PLA composite cast films and thermoformed films containing various untreated filler contents obtained from a second heating dynamic DSC scan

Sample code	ϕ_F [a] (vol%)	$T_{g\,PLA}$ (°C)	T_{cc} (°C)	T_m (°C)	ΔH_{cc} (J/g)	ΔH_m (J/g)	X_c (%)	
							Cast	Thermoform
Neat PLA	0	58.8	125.9	149.7	4.6	7.77	3.3	9.3
Talc1	1	58.8	102.8	144.4/151.2	13.2	20.5	7.9	12.8
Talc3	3	58.5	100.5	144.1/151.3	14.4	22.7	9.2	14.7
Talc5	5	58.6	100.1	145.8/152.6	18.5	29.5	12.5	18.6
Talc7	7	58.8	98.5	145.4/152.1	18.8	29.7	12.7	20.1
Talc10	10	58.7	99.5	144.8/152.4	19.2	30.2	13.2	22.3
$CaCO_3$1	1	58.8	109.3	146.2/152.0	21.2	26.3	5.5	8.0
$CaCO_3$3	3	58.8	110.8	146.3/149.7	19.9	26.3	7.1	10.9
$CaCO_3$5	5	58.7	111.9	146.6/153.7	22.1	30.1	9.1	14.2
$CaCO_3$7	7	58.8	110.5	145.5/150.9	19.3	27.9	10.0	16.6
$CaCO_3$10	10	58.9	110.3	146.2/151.6	18.3	27.4	10.9	17.4
Starch1	1	58.7	119.4	149.2	20.3	24.2	4.2	6.3
Starch3	3	58.7	119.1	149.7	19.2	24.7	6.1	7.9
Starch5	5	58.6	118.2	151.2	20.7	26.2	6.2	10.1
Starch7	7	58.7	117.9	150.2	20.5	26.6	7.1	12.2
Starch10	10	58.6	117.6	149.5	20.9	27.6	8.1	14.0

[a] ϕ_F is filler content

fine layer of conductive gold to increase contrast and reduce charging prior to examination.

Tensile properties including tensile strength, elongation-at-break, Young's modulus, and tensile toughness of cast films and thermoformed films of neat PLA and PLA composites were measured at room temperature using a universal testing machine (Intron model 5567, USA) in accordance with ASTM D882. Load cell was 1 kN and crosshead speed was 12.5 mm/min. Ten specimens with a rectangular shape (10 mm × 100 mm) were cut from the cast films and thermoformed films to obtain the mean value of each formula.

Thermal properties and isothermal cold crystallization behavior of the neat PLA and PLA composites were investigated using differential scanning calorimetry (Perkin Elmer, Diamond DSC, USA) under a nitrogen flow rate of 50 mL/min to avoid thermal degradation. About 10 mg of samples from cast films and thermoformed films were sealed in 50 µL standard aluminum pan. Baseline was recorded using an empty aluminum pan.

For dynamic DSC measurement, samples were heated from room temperature to 190 °C at a heating rate of 10 °C/min and maintained at this temperature for 5 min to erase thermal history. Afterwards, the samples were cooled down to room temperature at a cooling rate of 10 °C/min and secondly heated to 190 °C at a heating rate of 10 °C/min. The thermal transition temperatures and enthalpies were recorded from the second heating scan. Thermal transition temperatures included glass transition temperature (T_g), cold crystallization temperature (T_{cc}), and melting temperature (T_m). Degree of crystallinity (X_c) was calculated using the following equation:

$$X_c(\%) = \frac{\Delta H_m - \Delta H_{cc}}{\left(\Delta H_m^0 \times w\right)} \times 100 \quad (1)$$

where, ΔH_m is enthalpy of melting and ΔH_{cc} is enthalpy of cold crystallization. $\Delta H_m{}^0$ is the enthalpy of melting of totally crystallized PLA (93 J/g) [26]. Weight fraction of PLA in the composites is denoted as *w*.

For the studies on isothermal cold crystallization kinetics, the samples were heated from room temperature to the predetermined isothermal temperatures (T_{iso}) at 90 °C, 100 °C, 110 °C, 120 °C and 130 °C at a heating rate of 80 °C/min. The development of exothermic heat flow under isothermal condition was recorded. Finally, the isothermally crystallized samples were further heated to 190 °C at a heating rate of 10 °C/min to evaluate the degree of crystallinity in annealed PLA composites.

Results and discussion

Characterization of filler functionalized by silane coupling agent

Surface treatment of inorganic filler to covalently attach new functional groups onto its surface has extensively been performed to enhance the performance of the polymer composites. Among various methods, silanization has been widely used because the reaction is simple, low-cost, and effective for the filler surface with rich hydroxyl groups. The mechanism of the surface treatment with silane coupling agent is illustrated in Scheme 1. The ethoxy groups (−OEt) of silane coupling agent were hydrolyzed, forming silanol-containing species which can further react with the hydroxyl groups on the surface of the inorganic fillers via condensation. Finally, the modified filler surface with new reactive functional groups (*R*) was obtained. It is worth mentioning that the silanization is in general performed in acidic condition to not only help the hydrolysis reaction of silane, but also hinder the self-condensation of hydrolyzed silanols [25]. In this research, aminopropyl and vinyl were the reactive organo-functional groups of silane coupling agent.

The surface chemistry of the untreated talc and talc treated with 3-aminopropyltriethoxysilane (APTES) and vinyltriethoxysilane (VTES) was examined using FTIR measurement as displayed in Fig. 1. The simple formula of the untreated talc was $Mg_3Si_4O_{10}(OH)_2$ and its FTIR spectra showed Si–OH stretching vibration at 3645 cm^{-1}, Si–O asymmetric stretching at 984 cm^{-1} and Si–O symmetric bending at 669 cm^{-1}. As demonstrated in Scheme 1, the silanol group at 3645 cm^{-1} mainly disappeared after silanization and the new bond of Si–O–Si was formed as can be detected in the sharp absorption bands at 1127 cm^{-1}

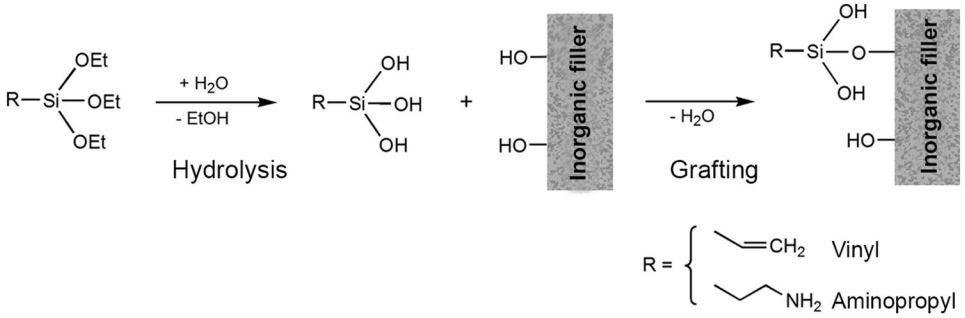

Scheme 1 Mechanism of surface functionalization of inorganic filler by silane coupling agent

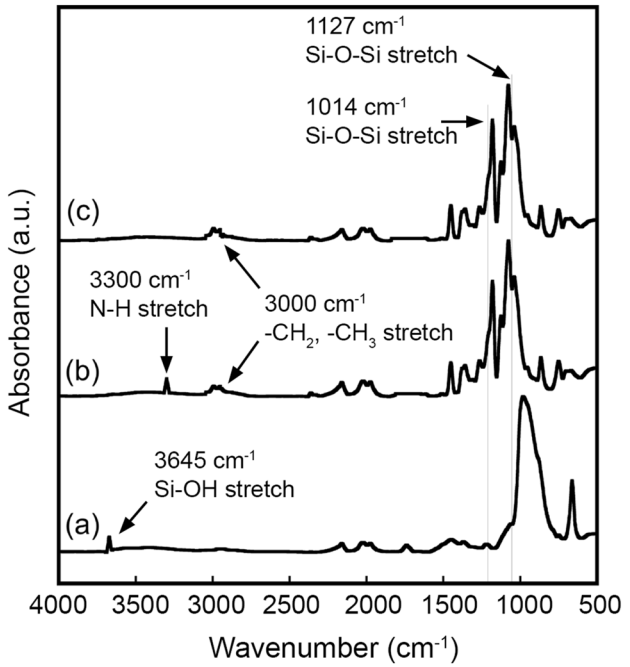

Fig. 1 FTIR spectra of **a** untreated talc particles, and talc particles treated by **b** APTES and **c** VTES

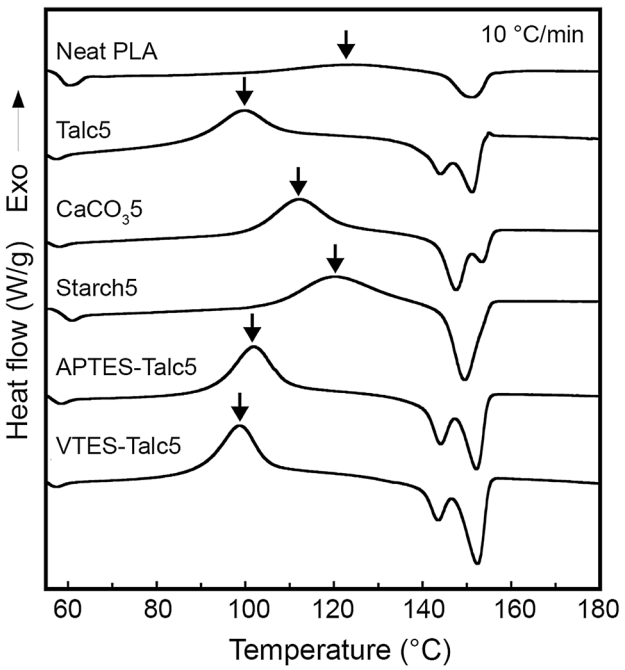

Fig. 2 Second heating dynamic DSC profiles of the neat PLA and PLA composite cast films containing 5 vol% fillers

(stretching) and 1014 cm^{-1} (bending). Further, the absorption band at 3000 cm^{-1} was noticed, which was attributed to $-CH_2$ and $-CH_3$ stretching vibration of silane coupling agent.

Although the vibration of C=C bond of vinyl group at 1600–1670 cm^{-1} was hardly seen in case of VTES-treated talc because the peak intensity was relatively weak, a peak of $-NH_2$ of aminopropyl chain around 3300 cm^{-1} was detected for APTES-treated talc. Accordingly, it can be summarized that the covalent grafting of silane coupling agent onto the talc surface was successful. The effect of silane coupling agent on the morphology, thermal and tensile properties of the PLA composites was discussed in the following sections.

Thermal behavior of PLA composites

The dynamic DSC thermograms and thermal properties that were obtained from the second heating scan of the neat PLA and PLA composite cast films are demonstrated in Fig. 2 and Table 1, respectively. It was found that the addition of untreated fillers at various contents did not affect the glass transition temperature (T_g) of PLA of the composites (~59 °C), indicating the immiscibility between PLA chains and these untreated filler particles. These results were also in agreement with the previous results in literature [13, 27, 28].

Besides, the exothermic cold crystallization enthalpy (ΔH_{cc}) increased and the cold crystallization temperature (T_{cc}) greatly reduced with the presence of untreated fillers. Namely, T_{cc} decreased from 126 to 100 °C for Talc5, 112 °C for $CaCO_3$5, and 118 °C for Starch5, implying that these fillers promoted the recrystallization of PLA chains upon heating, and talc powder was the most effective nucleating agent amongst them, which might be due to its surface activity as well as high specific surface area owing to its small particle size.

It was also found that T_{cc} of the composites seemed to be slightly reduced as filler content increased. For instance, T_{cc} values decreased about 3 °C as loading of untreated talc increased from 1 vol% to 10 vol%. The melting temperature (T_m) of the neat PLA was detected as a single peak at 150 °C. The DSC thermograms of the composites incorporated with talc and $CaCO_3$ showed the double melting peaks of PLA, which referred to the melting of PLA crystals having different crystal perfections [29, 30]. The lower melting temperature peak (T_{m1} ~ 144–147 °C) represented the disordered PLA crystalline structure. Upon further heating, this less perfect crystalline structure recrystallized into more perfect crystalline structure which subsequently melted at higher melting temperature (T_{m2} ~ 150–152 °C). This transition of disorder-to-order phase of PLA was also reported in other PLA systems [31, 32].

For PLA/untreated talc composites, talc can accelerate the cold crystallization of PLA better than $CaCO_3$ and cassava starch, respectively; thus, the more perfect PLA crystals were mainly formed resulting in the large area of

the endothermic melting peak T_{m2}. On the other hand, the PLA composites containing cassava starch showed only single endothermic peak T_{m1} because cassava starch had less effective nucleating ability for promoting PLA to crystallize upon heating, leading to formation of less perfect crystalline structure.

Finally, the degree of crystallinity (X_c) of the neat PLA and PLA composites is also summarized in Table 1. It was noticed that the neat PLA cast film was almost amorphous with X_c of 3%. The addition of filler significantly improved X_c of the composites and talc provided the highest X_c; this also confirmed the potential nucleating ability of talc to promote the crystallization of PLA upon heating from the glassy state (cold crystallization). For example, X_c values increased to 12.5%, 9.1%, and 6.2% for Talc5, $CaCO_3$5, and Starch5, respectively. Moreover, incorporating these fillers over 5 vol% seemed to enhance the degree of crystallinity insignificantly.

Dynamic DSC thermograms from the second heating scan of PLA composites containing 5 vol% untreated talc (Talc5) and silane-treated talc (APTES-Talc5 and VTES-Talc5) are also illustrated in Fig. 2 and their thermal properties are tabulated in Table 2. It was suggested that grafting of silane coupling agent onto the talc surface did not affect T_g of PLA in the composites. However, silane coupling agent chemically covered on the talc surface slightly changed T_{cc}. Namely, T_{cc} was 100.1 °C, 98.2 °C, and 101.4 °C for Talc5, APTES-Talc5, and VTES-Talc5, respectively; this revealed that grafted silane coupling agent can affect the cold crystallization behavior of PLA. As a consequence, the degree of crystallinity (X_c) changed from 12.5% for Talc5 to 17.8% for APTES-Talc5, and 14.7% for VTES-Talc5. As a consequence, the isothermal cold crystallization kinetics was investigated for neat PLA and the PLA composites containing 5 vol% fillers, which will be described in the following section.

Isothermal cold crystallization kinetics of PLA composites

The effect of untreated talc, $CaCO_3$, cassava starch, APTES-treated talc, and VTES-treated talc on the isothermal cold crystallization kinetics of the PLA composites was investigated in the isothermal cold crystallization temperature (T_{iso}) of 90–130 °C, as displayed in Fig. 3. Note that the cold crystallization time was recorded when the temperature measured from DSC program was equal to the setting isothermal temperature. All DSC thermograms showed the smooth bell-shaped curves.

The normalized exothermic heat flow sharply developed at the beginning of the DSC measurement owing to the fact that the PLA chains nucleated into the small PLA crystallites and then grew. After a period of crystallization time, the PLA crystallites became larger and collided with the adjacent crystallites, inhibiting the crystal growth process. As a result, the development rate of the normalized exothermic heat flow subsequently slowed down until the normalized exothermic heat flow reached the baseline, which was an indicative of the finished crystallization process.

Maximum cold crystallization time (t_{max}), which was the crystallization time at the highest normalized heat flow, was the lowest at T_{iso} range of 100–110 °C. Lower t_{max} indirectly indicated faster cold crystallization rate.

In principle, the optimal crystallization rate was acquired at the temperature between glass transition temperature (T_g) and melting temperature (T_m) of the polymer [33]. Below T_g, polymer was in the glassy state in which the segmental motion of the polymer chains did not occur and polymer chains had a stable structure macroscopically. This was the reason why the overall crystallization time, which was the time required to complete the cold crystallization process (heat flow of DSC thermogram was back to baseline), and t_{max} for the sample measured at $T_{iso} = 90$ °C were lower than $T_{iso} = 100$ °C.

On the other hand, Above T_m, the structure of polymer chains was unstable owing to the thermal atomic vibration disrupting the molecular orientation, thus polymer chains cannot nucleate and form the orderly crystalline form. As T_{iso} was closed to T_m, the normalized heat flow became broader and the overall crystallization time was prolonged. For instance, the overall crystallization time of the neat PLA increased from 10 to 40 min when T_{iso} changed from 100 to 130 °C. Particularly, the heat flow exhibited a delay of initial crystallization development for the neat PLA and PLA/cassava starch composites at $T_{iso} = 130$ °C because the nucleation rate was very slow.

The normalized exothermic heat flow from Fig. 3 can be converted into the development of relative degree of crystallinity as can be seen in Fig. 4. The degree of crystallinity X_c was calculated using the following equation:

Table 2 Thermal properties of the PLA composites containing treated filler obtained from second heating dynamic DSC scan

Sample code	$T_{g\ PLA}$ (°C)	T_{cc} (°C)	T_m (°C)	ΔH_{cc} (J/g)	ΔH_m (J/g)	X_c (%)	
						Cast	Thermoform
U-Talc5	58.6	100.1	145.8/152.6	18.5	29.5	12.5	18.6
APTES-Talc5	58.1	098.2	146.2/154.2	21.5	37.2	18.3	27.2
VTES-Talc5	58.4	101.4	145.5/152.7	19.2	32.2	14.1	20.7

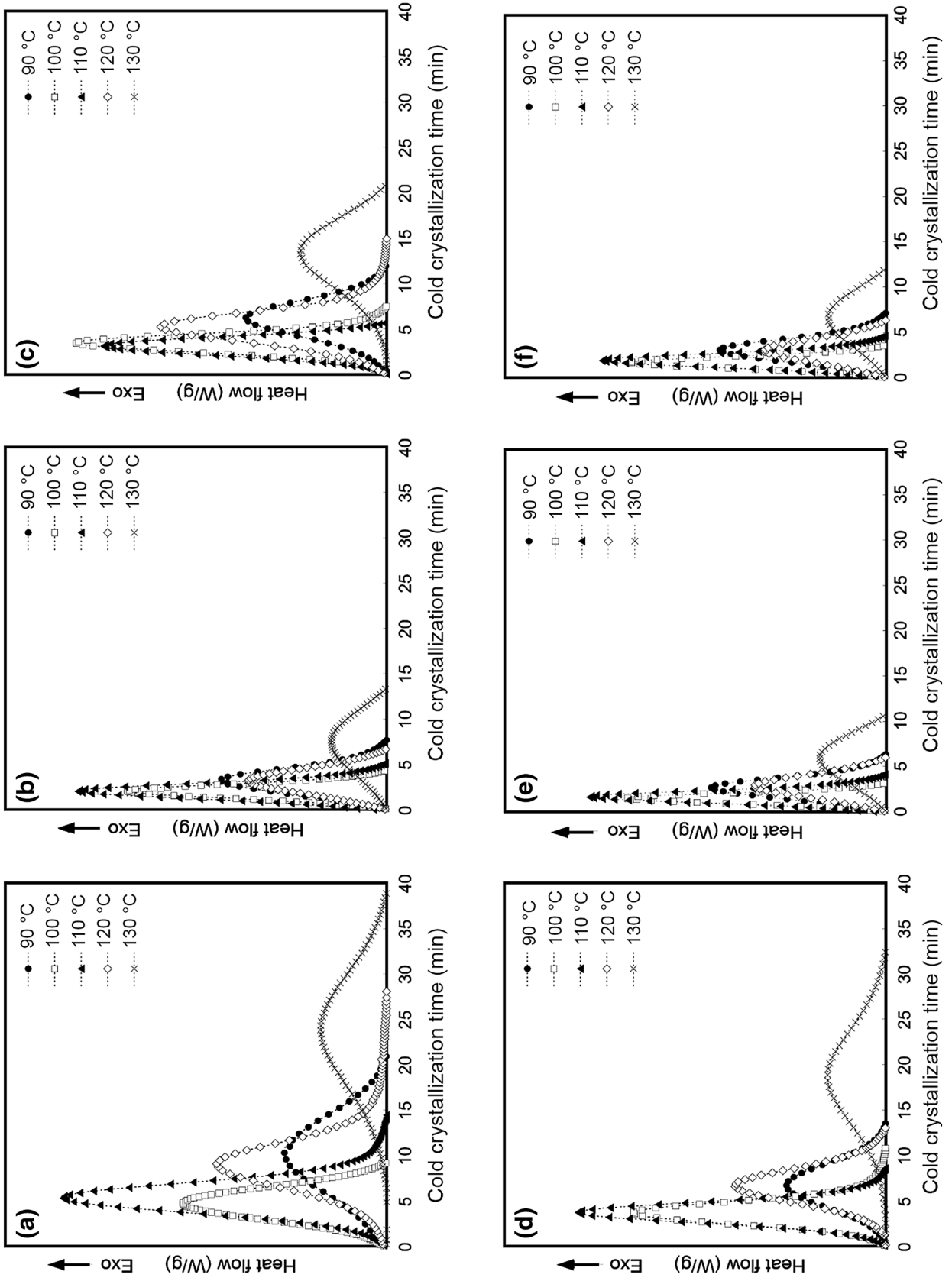

Fig. 3 DSC isothermal cold crystallization thermograms of **a** neat PLA, **b** Talc5, **c** $CaCO_3$5, **d** Starch5, **e** APTES-Talc5, and **f** VTES-Talc5 samples

Table 3 Isothermal cold crystallization kinetics parameters of the PLA composite cast films containing treated filler at $T_{iso} = 100$ °C

Sample code	T_{iso} (°C)	Avrami index n	k (min^{-n})	$t_{1/2,fit}$ (min)	$t_{1/2,exp}$ (min)	t_{max} (min)	R^2
U-Talc5	100	3.1	4.32×10^{-2}	2.4	2.2	1.9	0.9996
APTES-Talc5	100	3.2	1.93×10^{-1}	1.5	1.7	1.5	0.9995
VTES-Talc5	100	3.1	6.21×10^{-2}	2.2	2.0	1.8	0.9997

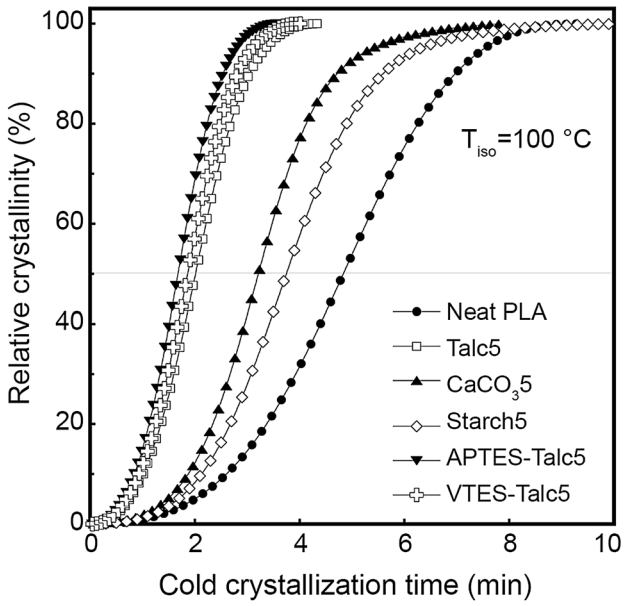

Fig. 4 Development of relative degree of crystallinity X_c of the neat PLA and PLA composite cast films containing 5 vol% fillers at $T_{iso} = 100$ °C (Horizontal line is $X_c = 50\%$)

$$X_c = \frac{X_c(t)}{X_c(t=\infty)} = \frac{\int_0^t \cdot \frac{dH(t)}{dt} dt}{\int_0^\infty \cdot \frac{dH(t)}{dt} dt} \quad (2)$$

where, $H(t)$ is the normalized heat flow from the DSC thermograms. X_c is the ratio of degree of crystallinity after cold crystallization time t ($X_c(t)$) to the total degree of crystallinity after completion of crystallization [$X_c(t=\infty)$]. The slow development of X_c at the early stage was related to the formation of small PLA nuclei. At the middle stage of cold crystallization, X_c was developed linearly, implying that the crystal growth rate of PLA was independent of the degree of its crystallinity.

Eventually, the X_c development gradually slowed down due to the impingement of PLA crystals with the adjacent ones, stopping the crystal growth process. The experimental cold crystallization half time ($t_{1/2,exp}$) was the time necessary for the polymer chains to crystallize half of the total degree of crystallinity ($X_c = 50\%$). Similar to the t_{max} results from Fig. 3, $t_{1/2,exp}$ values of the neat PLA and its composites at 100 °C increased in the following order: APTES-Talc5, VTES-Talc5, Talc5, $CaCO_3$5, Starch5, and neat PLA, which confirmed that talc particles with the surface treatment by silanization gave the fastest cold crystallization rate.

According to the linear relationship between growth rate of the polymer crystals and the crystallization time under isothermal condition, the Avrami model [34] can be used to study the crystallization kinetics of polymer at a constant temperature and it can be expressed in the following equation:

$$1 - X_c = \exp(-kt^n) \quad (3)$$

By taking the double logarithm of Eq. (3), the linear relationship can be expressed as follows:

$$\log\left[-\ln(1 - X_c)\right] = \log(k) + n\log(t) \quad (4)$$

where, k is the temperature–dependent isothermal cold crystallization rate constant and n is the Avrami index. Following Lorenzo et al. [35] who suggested the guidelines for the use of Avrami equation for the isothermal crystallization kinetics studies, it was important to point out that the range of X_c data for fitting with Avrami equation should be chosen between 3 and 80% to obtain the reliable isothermal kinetics information because of the inaccurate experimental data resulting from the unsteady DSC measurement ($X_c < 3\%$) as well as the deviation from linearity of crystal growth rate of PLA owing to the secondary crystallization process ($X_c > 80\%$).

Figure 5 shows the graph plotting of $\log[-\ln(1 - X_c)]$ against $\log(t)$ following Eq. (4). The slope is Avrami index n and the y-interception is $\log(k)$. The straight lines in Fig. 5 are the linear fittings of Avrami model with experimental data. It is showed in Table 3 that large coefficient of determination ($R^2 > 0.99$) was achieved, that indicated the Avrami equation was valid for the isothermal cold crystallization kinetics study in this work.

Another crucial isothermal crystallization kinetics parameter was the crystallization half time ($t_{1/2}$). Beside the experimental crystallization half time $t_{1/2,exp}$ that can be obtained from Fig. 4, the crystallization half time obtained by Avrami fitting $t_{1/2,fit}$ can also be calculated using the following equation:

$$t_{1/2,fit} = (\ln 2/k)^{1/n} \quad (5)$$

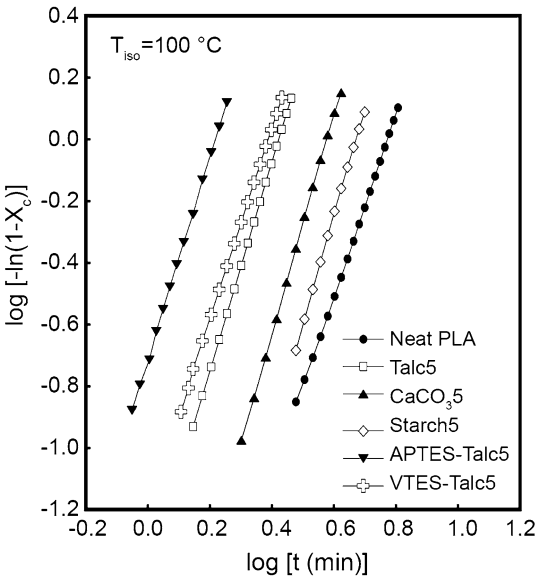

Fig. 5 Avrami plots of the neat PLA and PLA composite cast films containing 5 vol% fillers at T_{iso} = 100 °C (Symbol shows experimental result and solid lines are Avrami fitting)

where, k and n are isothermal cold crystallization rate constant and Avrami index, respectively, acquired by fitting the experimental data with Avrami model.

All isothermal cold crystallization kinetics parameters, i.e., Avrami index n, cold crystallization rate constant k, crystallization half times acquired from the experimental data $t_{1/2,exp}$ and from the Avrami fitting $t_{1/2,fit}$, and maximum crystallization time t_{max}, of the neat PLA and its composites containing 5 vol% fillers are tabulated in Table 3. It was mentioned that the isothermal cold crystallization kinetics parameters were strongly sensitive to T_{iso} value. As T_{iso} value is closed to that of T_m of PLA (i.e., T_{iso} = 130 °C), the polymer chain orientation and nucleation formation are disrupted by the high thermal energy, resulting in slowing down of cold crystallization that was evidenced by decreased k values and increased $t_{1/2}$ values. For instance, k values of Talc5 were 3.40×10^{-2}, 4.32×10^{-2}, 3.25×10^{-2}, 2.71×10^{-2}, and 8.56×10^{-3} min^{-1} at T_{iso} = 90 °C, 100 °C, 110 °C, 120 °C, and 130 °C, respectively. Comparing the samples at the same T_{iso} value, APTES-Talc5 gave the shortest $t_{1/2}$ and t_{max} values as well as the highest k value, meaning that the rate of cold crystallization was the fastest and talc treated by APTES was the most effective nucleating agent for cold crystallization process of PLA in this research. Avrami index n implied the geometric dimensionality of the growing crystals (1 represented one-dimensional rod-like crystal growth, 2 represented two-dimensional lamellar growth, and 3 represented three-dimensional spherulitic growth) as well as, for the time dependence of nucleation (0 referred to instantaneous nucleation and 1 referred to sporadic nucleation). Moreover, the non-integer n value implied the spherulitic growth from a mixture of instantaneous and sporadic nuclei condition.

Table 4 Isothermal cold crystallization kinetics parameters of the neat PLA and PLA composites containing untreated fillers at various T_{iso}

Sample code	T_{iso} (°C)	Avrami index n	k (min^{-n})	$t_{1/2,fit}$ (min)	$t_{1/2,exp}$ (min)	t_{max} (min)	R^2
Neat PLA	90	2.6	1.55×10^{-3}	10.5	9.1	9.9	0.9984
	100	2.9	5.43×10^{-3}	5.3	4.6	4.5	0.9994
	110	3.7	9.30×10^{-4}	6.0	5.2	5.1	0.9993
	120	3.9	8.85×10^{-5}	10.0	8.8	9.2	0.9986
	130	3.4	1.22×10^{-5}	25.1	24.0	23.2	0.9991
Talc5	90	2.8	3.40×10^{-2}	2.9	3.3	3.2	0.9997
	100	3.1	4.32×10^{-2}	2.4	2.2	1.9	0.9996
	110	3.3	3.25×10^{-2}	2.5	2.0	2.0	0.9999
	120	2.9	2.71×10^{-2}	3.5	3.2	3.1	0.9999
	130	2.5	8.56×10^{-3}	6.8	6.2	7.3	0.9997
$CaCO_3$5	90	3.2	2.70×10^{-3}	5.7	5.3	5.8	0.9998
	100	3.6	8.71×10^{-3}	3.4	3.2	3.2	0.9999
	110	3.7	3.95×10^{-3}	4.0	3.4	3.1	0.9997
	120	3.8	6.56×10^{-4}	6.2	5.3	5.2	0.9991
	130	3.1	2.12×10^{-4}	13.6	13.4	13.2	0.9999
Starch5	90	3.4	8.90×10^{-4}	7.1	6.5	6.8	0.9997
	100	3.5	4.50×10^{-3}	4.2	3.7	3.5	0.9998
	110	3.6	2.76×10^{-3}	4.6	4.0	3.6	0.9997
	120	3.9	9.13×10^{-5}	8.8	8.0	7.0	0.9994
	130	3.7	4.13×10^{-5}	13.9	15.8	18.0	0.9980

In this work, the Avrami index n values were 3.3, 3.0, 3.4, and 3.6 for the neat PLA, Talc5, $CaCO_3$5, and Starch5, respectively, which lied in the similar range suggesting that the addition of untreated fillers showed the three-dimensional spherulitic growth of PLA with a mixture of instantaneous and sporadic nuclei. Moreover, the n values most likely tended to increase from 3.0 to 4.0 as T_{iso} value increasing, inferred the transition from heterogeneous nucleation to homogeneous nucleation [36, 37].

Although the Avrami index n of the composites comprised of untreated and treated talc particles had the same value ($n \sim 3.1$) which reflected that silane coupling agent did not significantly effect on the nucleation and growth mechanisms of PLA, the cold crystallization rate was fastened as a result of modified surface functionality on the talc particles' surface. For instance, cold crystallization rate constant k values of the PLA composites were 4.32×10^{-2}, 1.93×10^{-1}, and 6.21×10^{-2} min^{-1} and Avrami fitted crystallization half time $t_{1/2,fit}$ values were 2.4, 1.5, 2.2 min for Talc5, APTES-Talc5, and VTES-Talc5, respectively as shown in Table 4. Hence, these results revealed that the aminopropyl groups of APTES had more potential to improve the isothermal cold crystallization rate of PLA composites than the vinyl groups of VTES. For surface treatment, the enhancement of cold crystallization acceleration might be due to the strong interaction between surface of talc particles and polymer matrix and its good dispersion in the PLA matrix, as similarly reported elsewhere in other polymer composite systems [17, 38].

Morphology of PLA composites

Figure 6a–f illustrate the SEM micrographs of the cross-sectional cryofractured surfaces of PLA composite cast films containing 5 vol% untreated talc, $CaCO_3$, cassava starch, APTES-treated talc, and VTES-treated talc, respectively. These PLA composites were classified as Talc5, $CaCO_3$5, Starch5, APTES-Talc5, and VTES-Talc5, respectively. Cryofractured surface of the neat PLA film was smooth (Fig. 6a).

Talc5 sample in Fig. 6b exhibited a uniform dispersion of plate-like talc particles in the PLA matrix; however, some untreated talc particles were pulled out upon cryofracturing step letting voids remained on the fractured surface as can be seen in drew circles in Fig. 6b. Even though untreated

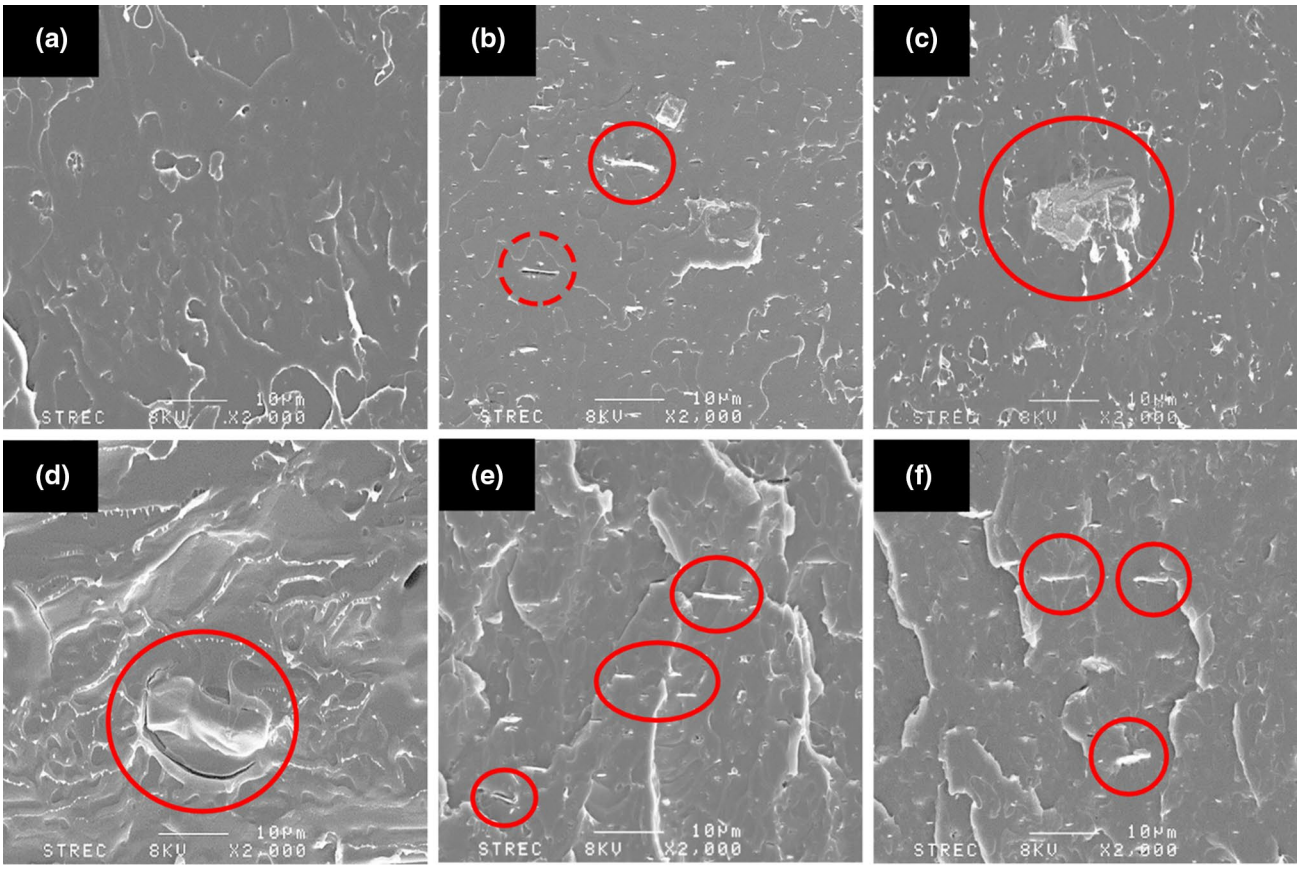

Fig. 6 SEM micrographs of cross-sectional cryofractured surfaces of the cast films of **a** neat PLA, **b** Talc5, **c** $CaCO_3$5, **d** Starch5, **e** APTES-Talc5, and **f** VTES-Talc5 samples (Inserted circles indicate filler particles)

talc particles' surfaces were hydrophobic which made them dispersed well in the PLA matrix, the pull-out phenomenon of untreated talc particles shown on the fractured surface was also reported elsewhere [31].

In the material specification sheet, the mean particle size of $CaCO_3$ particles was approximately 5 μm. However, the $CaCO_3$ particle in Fig. 6c was significantly larger, referring to the aggregation of $CaCO_3$ particles. Moreover, Fig. 6d revealed the debonding at the interface of starch particles and PLA matrix. These SEM results suggested the weak interfacial adhesion and incompatibility between these fillers and PLA matrix.

For the SEM micrographs of the PLA composites composed of silane-treated talc particles (Fig. 6e–f), the pulled-out phenomenon of silane-treated talc particles from the PLA matrix was rarely observed which was attributed to the improvement of the interfacial interaction and stronger interfacial strength between PLA matrix and reactive silane functional groups on the talc particles' surfaces. The silane-treated talc particles were still intact and adhered to the cryofractured surfaces of APTES-Talc5 and VTES-Talc5 samples as illustrated in Figs. 6e–f.

PLA has strong hydrophobicity. Modifying the talc particles' surfaces with VTES will impart hydrophobic vinyl groups in place of hydrophilic hydroxyl groups; which enhanced the affinity of treated talc particles with PLA chains through the van der Waals interactions. For PLA/APTES-treated talc composites, amino group ($-NH_2$) of APTES can show strong hydrogen-bonding interaction or chemically react with −OH and −COOH terminal groups of PLA.

The enhancement of adhesion between treated talc particles and PLA matrix was responsible for good dispersion in conjunction with less debonding of talc particles compared with the PLA/untreated talc composites. This interfacial interaction improvement in the polymer composites containing silane-treated fillers have been reported in literature. Huda and coworkers [39] reported that the PLA hybrid composites containing silane-treated talc and recycled newspaper cellulose fibers showed good dispersion of the talc particles and strong adhesion between them and polymer matrix, as well as, high flexural modulus and flexural strength compared with the untreated systems.

Tensile properties of PLA composites

The tensile properties, i.e., tensile strength, Young's modulus, elongation-at-break, and tensile toughness, of cast films and thermoformed films for the neat PLA and PLA composites containing 5 vol% fillers are shown in Fig. 7. Although the elongation-at-break values did not significantly differed for these samples which was about 3%, the addition of filler increased tensile strength and Young's modulus, as well as, slightly reduced toughness in comparison with those of the unfilled PLA. This was due to the reinforcing effect of filler aiding the load transfer from polymer matrix to the filler particles across the interface.

It is known that the reinforcement in the polymer composites strongly depended on the characteristics of the polymer (e.g., crystallinity, stereoregularity, and degree of polymerization), characteristics of the filler (e.g., size, geometry, and volume fraction), and polymer/particle interfacial adhesion [40]. Among these untreated fillers, the PLA composites composed of talc particles provided the highest tensile strength and tensile modulus. Comparing to the neat PLA cast films, the incorporation of 5 vol% talc particles increased the tensile strength (from 42.8 to 50.2 MPa) and Young's modulus (from 1797 to 2198 MPa). These results were in an agreement with the works done by Battegazzore et al. [27] and Shakoor and Thomas [31] who reported the tensile modulus and storage modulus improvements of the PLA/talc composites.

Additionally, it was found that functionalization of talc particles with silane coupling agent can further increase the tensile strength and tensile modulus of the PLA composites. As can be seen from the SEM micrographs in Fig. 6, silanization of the talc particles improved their interfacial adhesion with PLA matrix, as evidenced by less debonded talc particles from the cryofractured surfaces. This interfacial adhesive strength resulted in a better load transfer across the interface during the tensile testing.

It was also detected that APTES-Talc5 film showed higher tensile strength and Young's modulus than VTES-Talc5 film. The vinyl group of VTES increased the hydrophobicity of talc particles, leading to an increased affinity and increased physical intermolecular forces between talc particles and PLA matrix. On the other hand, the amine groups ($-NH_2$) of APTES can both hydrogen-bonded or covalently bonded with the terminal hydroxyl (−OH) and carboxyl (−COOH) functional groups of PLA, which were considerably stronger than the physical interaction in the case of VTES treatment. From this reason, APTES treatment showed higher tensile strength and tensile modulus than VTES treatment.

The improvement of mechanical properties due to the silane coupling agent has also been reported by many researchers. Eng et al. [20] reported the increase in flexural modulus, tensile strength and modulus, and impact strength when incorporated methacrylate silane-treated oil palm mesocarp fiber into the PLA/polycaprolactone hybrid composites owing to the effect of fiber/matrix interaction. Moreover, Sibeko and Luyt [21] found the improvement in thermal and tensile properties of the vinyl silane cross-linked low density polyethylene composites containing nanoclay particles as a result of enhancement in degree of clay dispersion and interfacial interaction.

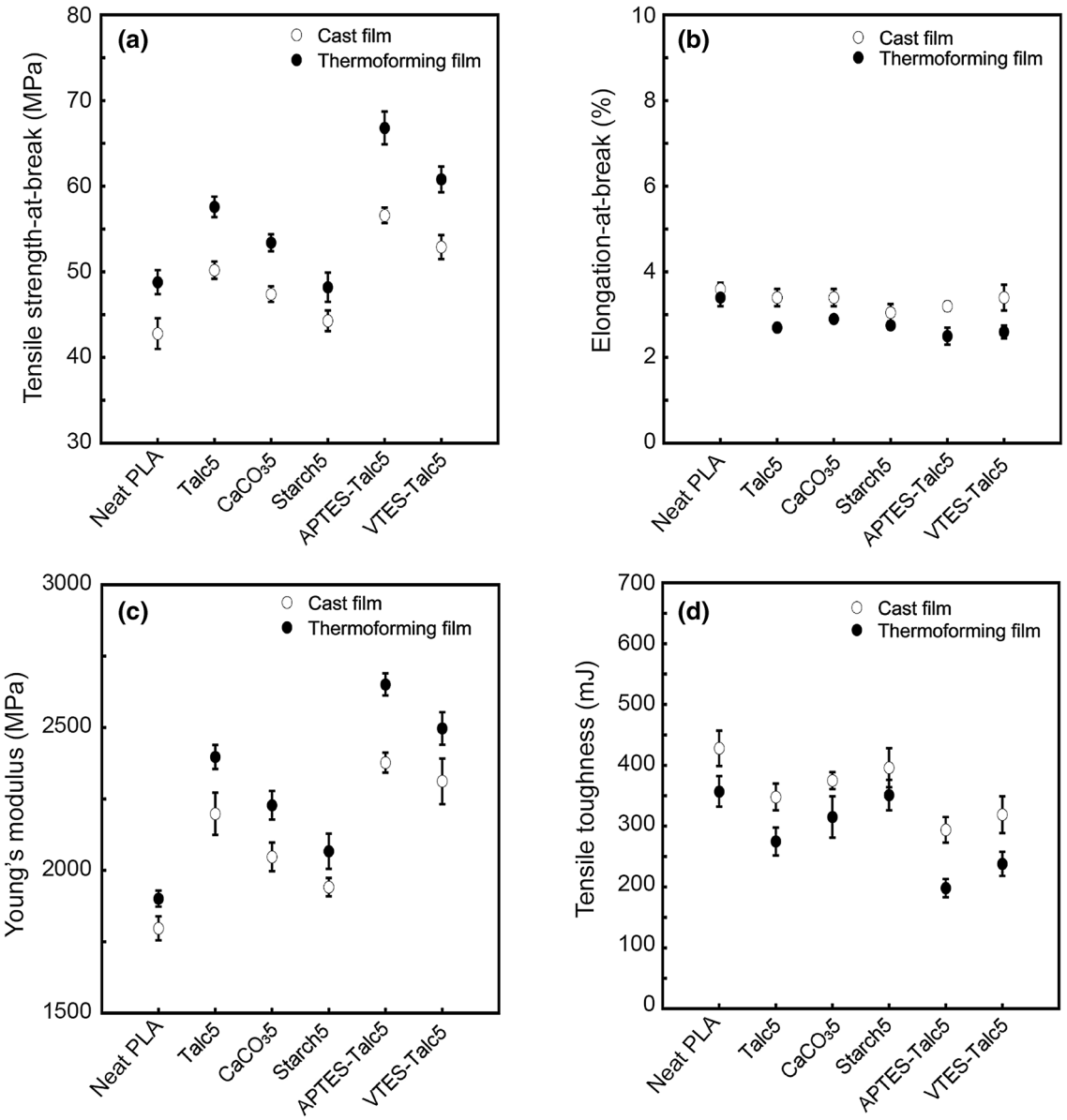

Fig. 7 Tensile properties of the neat PLA and PLA composite cast films and thermoformed films containing 5 vol% fillers: **a** tensile strength-at-break, **b** elongation-at-break, **c** Young's modulus, **d** tensile toughness

Beside the interfacial adhesion improvement mentioned earlier, the difference in degree of crystallinity also affected the tensile properties of the PLA composites. The cast films of the neat PLA and PLA composites were isothermally annealed to investigate the effect of annealing process on thermal and tensile properties. Herein, annealing temperature was the isothermal cold crystallization temperature that gave the fastest crystallization rate, which was 100 °C for all samples.

Moreover, the annealing time was the overall crystallization time until the cold crystallization finished as presented in Fig. 3. Hence, annealing time was varied depending on the composite system. The annealing times of the neat PLA, Talc5, $CaCO_3$5, Starch5, APTES-Talc5, and VTES-Talc5 at 100 °C were 9.0, 4.0, 7.5, 11.0, 2.8, and 3.5 min, respectively. After annealing process, the tensile properties were significantly changed for all composites. For instance, thermoformed films of Talc5 exhibited an enhancement of tensile strength (57.6 MPa) and Young's modulus (2397 MPa). This can be explained by the fact that annealing of the cast films under isothermal cold crystallization between T_g and T_m of PLA induced the orientation of PLA molecular chains, as well as, eliminated the existence of crystal defects, leading to an increased degree of crystallinity [41].

By testing the samples prior to and after annealing process by dynamic DSC scan, the degree of crystallinity of PLA in the composites increased from cast films to thermoformed films as shown in Tables 1 and 2. The degree of crystallinity increased as follows: from 12.5 to 18.6% for Talc5, from 17.8 to 27.2% for APTES-Talc5, and from 14.7 to 20.7% for VTES-Talc5 thermoformed films. The highly ordered PLA crystalline structure was more difficult to break during tensile testing compared to the amorphous phase. Thus, it required higher force to deform the film specimens. It can be concluded that the improvements of tensile strength and tensile modulus were associated with the degree of crystallinity controlled by annealing, as well as, the degree of interfacial strength between filler particles and polymer matrix which related to the surface functionality of the filler.

Conclusions

The properties of the PLA composite films containing $CaCO_3$, cassava starch, untreated talc, and silane-treated talc particles with/without annealing were reported. Although the interfacial debonding and aggregation of untreated fillers from the SEM micrographs implied the weak interfacial interaction between untreated filler particles and PLA matrix, the presence of the incorporated untreated fillers enhanced the thermal properties and isothermal cold crystallization rate, particularly with the addition of talc particles. The fastest isothermal cold crystallization of PLA was acquired at 100 °C as confirmed by the highest cold crystallization rate constant k and the shortest crystallization half time $t_{1/2}$ values. Therefore, annealing of PLA composite cast films through the thermoforming process at this temperature can increase the crystallinity owing to the improved polymer chain orientation, leading to the enhanced tensile strength and Young's modulus. Furthermore, functionalization of talc particles with silane coupling agent provided stronger interfacial adhesion between talc particles and polymer matrix due to the interaction between functional groups of silane coupling agents grafted onto the talc particles' surfaces and terminal hydroxyl and carboxyl groups of PLA, which facilitated the affinity of the polymer chains and filler particles and promoted the crystallization of PLA. As a result, the isothermal cold crystallization rate and tensile strength and tensile modulus of PLA composites were additionally enhanced. Finally, it can be summarized that the intrinsic nature and surface functionality of filler played crucial roles in the crystallization and mechanical performance of the polymer composites.

Acknowledgements The authors sincerely acknowledge the financial support from the Ratchadaphisek Somphot Fund for Postdoctoral Fellowship, Chulalongkorn University, Thailand.

References

1. Di Lorenzo ML, Androsch R (2018) Industrial applications of poly(lactic acid). Springer, Cham
2. Sin LT, Tueen BS (2019) Polylactic acid: a practical guide for the processing, manufacturing, and applications of PLA. William Andrew, Oxford
3. Muller J, González-Martínez C, Chiralt A (2017) Combination of poly(lactic) acid and starch for biodegradable food packaging. Materials 10:E952. https://doi.org/10.3390/ma10080952
4. Alvarado N, Romero J, Torres A, Dicastillo CLD, Rojas A, Galotto MJ, Guarda A (2018) Supercritical impregnation of thymol in poly(lactic acid) filled with electrospun poly(vinyl alcohol)-cellulose nanocrystals nanofibers: development an active food packaging material. J Food Eng 217:1–10
5. Feng C, Yuan X, Chu K, Zhang H, Ji W, Rui M (2019) Preparation and optimization of poly(lactic acid) nanoparticles loaded with fisetin to improve anti-cancer therapy. Int J Biol Macromol 125:700–710
6. Singhvi MS, Zinjarde SS, Gokhale DV (2019) Polylactic acid: synthesis and biomedical applications. J Appl Microbiol 127:1612–1626. https://doi.org/10.1111/jam.14290
7. Huang T, Yamaguchi M (2017) Effect of cooling conditions on the mechanical properties of crystalline poly(lactic acid). J Appl Polym Sci 134:44960
8. Deetuam C, Samthong C, Pratumpol P, Somwangthanaroj A (2017) Improvement in morphology, mechanical and thermal properties of films produced by reactive blending of poly(lactic acid)/natural rubber latex with dicumyl peroxide. Iran Polym J 26:615–628
9. Auras RA, Lim L-T, Selke SEM, Tsuji H (2010) Poly(lactic acid): synthesis, structures, properties, processing, and applications. Wiley, New Jersey
10. Coppola B, Cappetti N, Di Maio L, Scarfalo P, Incarnato L (2018) 3D printing of PLA/clay nanocomposites: influence of printing temperature on printed samples properties. Materials 11:E1947. https://doi.org/10.3390/ma11101947
11. Abdallah W, Mirzadeh A, Tan V, Kamal MR (2019) Influence of nanoparticle pretreatment on the thermal, rheological and mechanical properties of PLA-PBSA nanocomposites incorporating cellulose nanocrystals or montmorillonite. Nanomaterials 9:E29. https://doi.org/10.3390/nano9010029
12. Lule Z, Kim J (2019) Nonisothermal crystallization of surface-treated alumina and aluminum nitride-filled polylactic acid hybrid composites. Polymers 11:E1077. https://doi.org/10.3390/polym11061077
13. Bher A, Unalan IU, Auras R, Rubino M, Schvezov CE (2018) Toughening of poly(lactic acid) and thermoplastic cassava starch reactive blends using graphene nanoplatelets. Polymers 10:95. https://doi.org/10.3390/polym10010095
14. Petchwattana N, Narupai B (2019) Synergistic effect of talc and titanium dioxide on poly(lactic acid) crystallization: an investigation on the injection molding cycle time reduction. J Polym Env 27:837–846
15. Nanthananon P, Seadan M, Pivsa-Art S, Hamada H, Suttiruengwong S (2018) Facile preparation and characterization of short-fiber and talc reinforced poly(lactic acid) hybrid composite with in situ reactive compatibilizers. Materials 11:E1183. https://doi.org/10.3390/ma11071183

16. Petchwattana N, Covavisaruch S, Petthai S (2014) Influence of talc particle size and content on crystallization behavior, mechanical properties and morphology of poly(lactic acid). Polym Bull 71:1947–1959
17. Tang H, Dong Q, Liu P, Ding Y, Wang F, Gao C, Zhang S, Yang M (2016) Isothermal crystallization of polypropylene/surface modified silica nanocomposites. Sci China Chem 59:1283–1290
18. Sabatini V, Farina H, Basilissi L, Silvestro GD, Ortenzi MA (2015) The use of epoxy silanes on montmorillonite: an effective way to improve thermal and theological properties of PLA/MMT nanocomposites obtained via "in situ" polymerization. J Nanomater. https://doi.org/10.1155/2015/418418
19. Nakamura Y, Nishida Y, Fukuda T, Fujii S, Sasaki M (2013) Mechanical properties of silane-treated silica particle-filled polyisoprene composites: influence of the alkoxy group mixing ratio in silane coupling agent containing. J Appl Polym Sci 128:2548–2555
20. Eng CC, Ibrahim NA, Zainuddin N, Ariffin H, Yunus WMZW (2014) Impact strength and flexural properties enhancement of methacrylate silane treated oil palm mesocarp fiber reinforced biodegradable hybrid composites. Sci World J. https://doi.org/10.1155/2014/213180
21. Sibeko MA, Luyt AS (2014) Preparation and characterization of vinylsilane crosslinked low-density polyethylene composites filled with nano clays. Polym Bull 71:637–657
22. Kusuktham B, Teeranachaideekul P (2014) Mechanical properties of high density polyethylene/modified calcium silicate composites. Silicon 6:179–189
23. Singha AS, Rana AK (2013) Effect of aminopropyltriethoxysilane (APS) treatment on properties of mercerized lignocellulosic *Grewia optiva* fiber. J Polym Environ 21:141–150
24. Li Q, Gao X, Cheng W, Han G (2017) Effect of modified red pottery clay on the moisture absorption behavior and weatherability of polyethylene-based wood-plastic composites. Materials 10:111. https://doi.org/10.3390/ma10020111
25. Salon MCB, Belgacem MN (2011) Hydrolysis-condensation kinetics of different silane coupling agents. Phosphorus Sulfur Silicon Relat Elem 186:240–254
26. Fischer EW, Sterzel HJ, Wegner G (1973) Investigation of the structure of solution grown crystals of lactide copolymers by means of chemical reactions. Kolloid Z Z Polym 251:980–990
27. Battegazzore D, Bocchini S, Frache A (2011) Crystallization kinetics of poly(lactic acid)-talc composites. Express Polym Lett 5:849–858
28. Shi N, Dou Q (2014) Crystallization behavior, morphology, and mechanical properties of poly(lactic acid)/tributyl citrate/treated calcium carbonate composites. Polym Compos 35:1570–1582
29. Zhang J, Tashiro K, Tsuji H, Domb AJ (2008) Disorder-to-order phase transition and multiple melting behavior of poly(*L*-lactide) investigated by simultaneous measurements of WAX and DSC. Macromolecules 41:1352–1357
30. Pan P, Zhu B, Kai W, Dong T, Inoue Y (2008) Polymorphic transition in disordered poly(*L*-lactide) crystals by annealing at elevated temperatures. Macromolecules 41:4296–4304
31. Shakoor A, Thomas NL (2014) Talc as nucleating agent and reinforcing filler in poly(lactic acid) composites. Polym Eng Sci 54:64–70
32. Samthong C, Deetuam C, Yamaguchi M, Praserthdam P, Somwangthanaroj A (2016) Effects of size and shape of dispersed poly(butylene terephthalate) on isothermal crystallization kinetics and morphology of poly(lactic acid) blends. Polym Eng Sci 56:258–268
33. Hoffman JD, David GT, Laurizten JI (1976) In: Treatise on solid state chemistry: crystalline and non-crystalline solid, N Hannay (ed), Plenum, New York
34. Avrami M (1940) Kinetics of phase change. II Transformation-time relations for random distribution of nuclei. J Chem Phys 8:212–225
35. Lorenzo AT, Arnal ML, Albuerne J, Müller AJ (2007) DSC isothermal polymer crystallization kinetics measurements and the use of the Avrami equation to fit the data: Guidelines to avoid common problems. Polym Test 26:222–231
36. Zhang J, Tsuji H, Noda I, Ozaki Y (2004) Structural changes and crystallization dynamics of poly(*L*-lactide) during the cold-crystallization process investigated by infrared and two-dimensional infrared correlation. Macromolecules 37:6433–6439
37. Anderson KS, Hillmyer MA (2006) Melt preparation and nucleation efficiency of polylactide stereocomplex crystallites. Polymer 47:2030–2035
38. Blagojević SL, Šturlić BZ, Igrec I (2013) Influence of silica nanofiller on the isothermal crystallization and melting of polyurethane elastomer. J Appl Polym Sci 129:1466–1475
39. Huda MS, Drzal LT, Mohanty AK, Misra M (2007) The effect of silane treated- and untreated-talc on the mechanical and physico-mechanical properties of poly(lactic acid)/newspaper fibers/talc hybrid composites. Compos B Eng 38:367–379
40. Friedrich K, Breuer U (2015) Multifunctionality of polymer composites: challenges and new solutions. William Andrew, New York
41. Auriemma F, Alfonso GC, Rosa CD (2017) Polymer crystallization I: From chain microstructure to processing. Springer, Cham